UMR 5131 CNRS

INTERNATIONAL FEDERATION OF AUTOMATIC CONTROL

1st IFAC Workshop on

FRACTIONAL DIFFERENTIATION and its APPLICATIONS

FDA'04

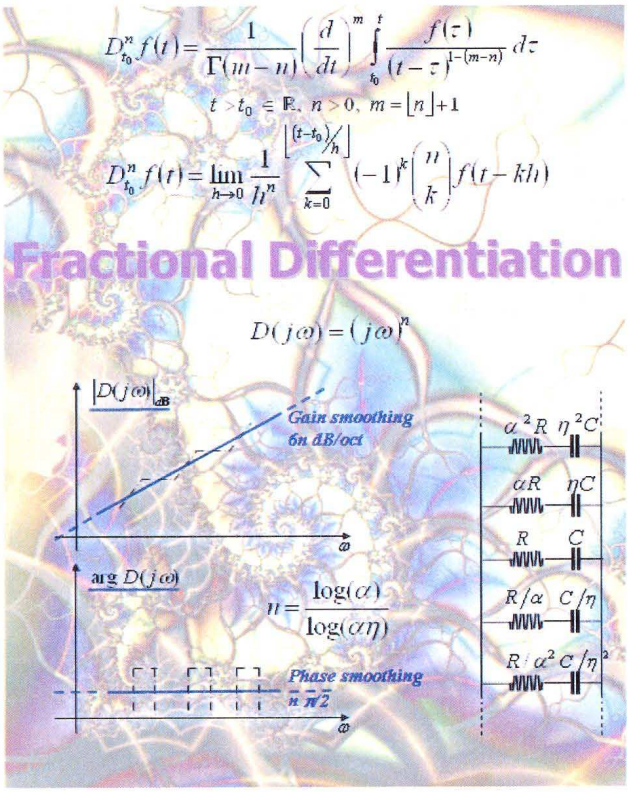

ENSEIRB, Bordeaux, France, July 19-21, 2004

WORKSHOP PREPRINTS/PROCEEDINGS N° 2004-1

UNIVERSITE BORDEAUX 1 Sciences Technologies

CNRS

ENSEIRB ECOLE NATIONALE SUPERIEURE ELECTRONIQUE, INFORMATIQUE & RADIOCOMMUNICATIONS BORDEAUX

HEXAPOD CONTROL THROUGH A FRACTIONAL ALGORITHM

Manuel F. Silva [*], J. A. Tenreiro Machado [*], António M. Lopes [+]

[*] *Department of Electrical Engineering, Institute of Engineering of Porto,*
Rua Dr. António Bernardino de Almeida, 4200-072 Porto, Portugal
Email: {mfsilva,jtm}@dee.isep.ipp.pt
[+] *Department of Mechanical Engineering, Faculty of Engineering of Porto,*
Rua Dr. Roberto Frias, 4200-465 Porto, Portugal
Email: aml@fe.up.pt

Abstract - This paper studies the performance of a Fractional Order controller in a hexapod robot with joint leg actuators having saturation. For that objective the robot prescribed motion is characterized in terms of several locomotion variables. Moreover, two indices measure the walking performance based on the mean absolute density of energy per travelled distance and on the hip trajectory errors. A set of experiments reveals the influence of the different controller tuning upon the proposed indices and on the feet trajectory tracking.

Keywords – Robotics, Walking, Control algorithms, Performance analysis

1. INTRODUCTION

Walking machines allow locomotion in terrain inaccessible to other type of vehicles, since they do not need a continuous support surface. On the other hand, the requirements for leg coordination and control impose difficulties beyond those encountered in wheeled robots (Song and Waldron, 1989). There exists a class of walking machines for which locomotion is a natural dynamic mode. Once started on a shallow slope, a machine of this class will settle into a steady gait, without active control or energy input (McGeer, 1990). However, the capabilities of these machines are quite limited. Previous studies focused mainly in the control at the leg level and leg coordination using neural networks (Tsai and Lee, 1998), fuzzy logic (Tsai, *et al*., 1997), central pattern generators (Collins and Richmond, 1994) and subsumption architecture (Celaya and Porta, 1995). There is also a growing interest in using insect locomotion schemes to control walking robots (Ferrell, 1995). In spite of the diversity of approaches, for multi-legged robots the control at the joint level is usually implemented through a simple *PID* like scheme with position/velocity feedback. Other approaches include sliding mode control (Martins-Filho, *et al*., 2003), computed torque control (Lee, *et al*., 1998) and hybrid force/position control (Song, *et al*., 1999).

The application of the theory of fractional calculus in robotics is still in a research stage, but the recent progress in this area reveals promising aspects for future developments (Silva, *et al*., 2003a).

With these facts in mind, a simulation model for multi-leg locomotion systems was developed, for several periodic gaits. Based on this tool, the present study compares different Fractional Order (*FO*) robot controller tuning. The analysis is based on the formulation of two indices measuring the mean absolute density of energy per travelled distance and the hip trajectory errors during walking. It is analysed the system performance for two cases: two leg joints are motor actuated and the ankle joint is mechanical actuated and the three leg joints are fully motor actuated. The simulations reveal the superior performance of the *FO* controller, with all leg joints motor actuated.

Bearing these facts in mind, the paper is organized as follows. Section two introduces the robot kinematic model and the motion planning scheme. Sections three and four present the robot dynamic model and control architecture and the optimizing indices, respectively. Section five develops a set of experiments that compare the performance of the different controller tuning. Finally, section six outlines the main conclusions and directions towards future developments.

2. ROBOT KINEMATICS AND TRAJECTORY PLANNING

We consider a walking system (Fig. 1) with $n = 6$ legs, equally distributed along both sides of the robot body, having each three rotational joints (*i.e.*, $j = \{1, 2, 3\} \equiv \{\text{hip, knee, ankle}\}$).

Motion is described by means of a world coordinate system. The kinematic model comprises: the cycle time T, the duty factor β, the transference time $t_T = (1-\beta)T$, the support time $t_S = \beta T$, the step length L_S, the stroke pitch S_P, the body height H_B, the maximum foot clearance F_C, the i^{th} leg lengths L_{i1} and L_{i2} and the foot trajectory offset O_i ($i = 1, \ldots, n$). Moreover, we consider a periodic trajectory for each foot, with body velocity $V_F = L_S / T$.

Gaits describe sequences of leg movements, alternating between transfer and support phases. Given a particular gait and duty factor β, it is possible to calculate, for leg i, the corresponding phase ϕ_i, the time instant where each leg leaves and returns to contact with the ground and the cartesian trajectories of the tip of the feet (that must be completed during t_T) (Song and Waldron, 1989). Based on this data, the trajectory generator is responsible for producing a motion that synchronises and coordinates the legs.

The robot body, and by consequence the legs hips, is assumed to have a desired horizontal movement with a constant forward speed V_F. Therefore, for leg i the cartesian coordinates of the hip of the legs are given by $\mathbf{p_{Hd}}(t) = [x_{iHd}(t), y_{iHd}(t)]^{\mathrm{T}}$:

$$\mathbf{p_{Hd}}(t) = [V_F t \quad H_B]^{\mathrm{T}} \tag{1}$$

Regarding the feet trajectories, on a previous work we evaluated two alternative space-time foot trajectories, namely a cycloidal and a sinusoidal function (Silva, *et al*., 2003b). It was demonstrated that the cycloid is superior to the sinusoidal function, because improves the hip and foot trajectory tracking, while minimising the corresponding joint torques. These results do not present significant changes for different acceleration profiles of the foot trajectory.

Considering the above conclusions, for each cycle the desired trajectory of the foot of the swing leg is computed through a cycloid function (Eq. 2). For example, considering that the transfer phase starts at $t = 0$ s for leg $i = 1$ we have for $\mathbf{p_{Fd}}(t) = [x_{iFd}(t), y_{iFd}(t)]^{\mathrm{T}}$:

- during the transfer phase:

$$\mathbf{p_{Fd}}(t) = \begin{bmatrix} V_F \left[t - \frac{T}{2\pi} \sin\left(\frac{2\pi t}{T}\right) \right] \\ \frac{F_C}{2} \left[1 - \cos\left(\frac{2\pi t}{T}\right) \right] \end{bmatrix} \tag{2}$$

- during the stance phase:

$$\mathbf{p_{Fd}}(t) = [V_F T \quad 0]^{\mathrm{T}} \tag{3}$$

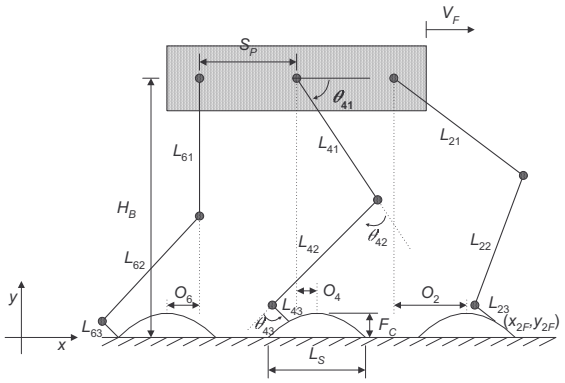

Fig. 1. Coordinate system and variables that characterize the motion trajectories of the multi-legged robot.

The algorithm for the forward motion planning accepts the desired cartesian trajectories of the leg hips $\mathbf{p_{Hd}}(t)$ and feet $\mathbf{p_{Fd}}(t)$ as inputs and, by means of an inverse kinematics algorithm $\boldsymbol{\psi}^{-1}$, generates the related joint trajectories $\boldsymbol{\Theta_d}(t) = [\theta_{i1d}(t), \theta_{i2d}(t), \theta_{i3d}(t)]^{\mathrm{T}}$, selecting the solution corresponding to a forward knee and a backward ankle:

$$\mathbf{p_d}(t) = [x_{id}(t) \quad y_{id}(t)]^{\mathrm{T}} \quad \mathbf{p_{Hd}}(t) \quad \mathbf{p_{Fd}}(t) \tag{4a}$$

$$\mathbf{p_d}(t) = \boldsymbol{\psi}(\boldsymbol{\Theta_d}(t)) \Rightarrow \boldsymbol{\Theta_d}(t) = \boldsymbol{\psi}^{-1}[\mathbf{p_d}(t)] \tag{4b}$$

$$\dot{\boldsymbol{\Theta}}_{\mathbf{d}}(t) = \mathbf{J}^{-1}[\dot{\mathbf{p}}_{\mathbf{d}}(t)], \quad \mathbf{J} = \frac{\partial \boldsymbol{\psi}}{\partial \boldsymbol{\Theta}} \tag{4c}$$

In order to avoid the impact and friction effects, at the planning phase we estimate null velocities of the feet in the instants of landing and taking off, assuring also the velocity continuity.

3. ROBOT DYNAMICS AND CONTROL ARCHITECTURE

3.1 Inverse Dynamics Computation

The planned joint trajectories constitute the reference for the robot control system. The model for the robot inverse dynamics is formulated as:

$$\boldsymbol{\Gamma} = \mathbf{H}(\boldsymbol{\Theta})\ddot{\boldsymbol{\Theta}} + \mathbf{c}(\boldsymbol{\Theta}, \dot{\boldsymbol{\Theta}}) + \mathbf{g}(\boldsymbol{\Theta}) + \mathbf{F_{RH}} + \mathbf{J_F^T}(\boldsymbol{\Theta})\mathbf{F_{RF}} \tag{5}$$

where $\boldsymbol{\Gamma} = [f_{ix}, f_{iy}, \tau_{i1}, \tau_{i2}, \tau_{i3}]^{\mathrm{T}}$ ($i = 1, \ldots, n$) is the vector of forces/torques, $\boldsymbol{\Theta} = [x_{iH}, y_{iH}, \theta_{i1}, \theta_{i2}, \theta_{i3}]^{\mathrm{T}}$ is the vector of position coordinates, $\mathbf{H}(\boldsymbol{\Theta})$ is the inertia matrix and $\mathbf{c}(\boldsymbol{\Theta}, \dot{\boldsymbol{\Theta}})$ and $\mathbf{g}(\boldsymbol{\Theta})$ are the vectors of centrifugal/Coriolis and gravitational forces/torques, respectively. The $n \times m$ ($m = 3$) matrix $\mathbf{J_F^T}(\boldsymbol{\Theta})$ is the transpose of the robot Jacobian matrix, $\mathbf{F_{RH}}$ is the $m \times 1$ vector of the body inter-segment forces and $\mathbf{F_{RF}}$ is the $m \times 1$ vector of the reaction forces that the ground exerts on the robot feet. These forces are null during the foot transfer phase. During the system simulation, Eq. (5) is integrated through the Runge-Kutta method.

Furthermore, we consider that the joint actuators are not ideal, exhibiting a saturation given by:

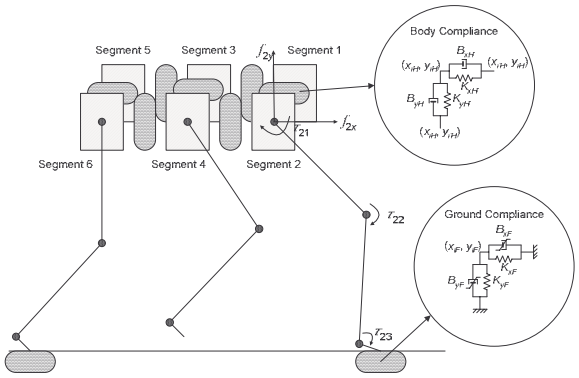

Fig. 2. Model of the robot body and foot-ground interaction.

$$\tau_{ijm} = \begin{cases} \tau_{ijC} & , \left|\tau_{ijC}\right| \le \tau_{ijMax} \\ \mathrm{sgn}\left(\tau_{ijC}\right) \cdot \tau_{ijMax} & , \left|\tau_{ijC}\right| > \tau_{ijMax} \end{cases} \quad (6)$$

where, for leg i and joint j, τ_{ijC} is the controller demanded torque, τ_{ijMax} is the maximum torque that the actuator can supply and τ_{ijm} is the motor effective torque.

3.2 Joint j = 3 Implementation

During this study leg joint $j = 3$ can be either mechanical actuated or motor actuated. For the mechanical actuated case, we suppose that there is a rotational spring-dashpot system connecting leg links L_{i2} and L_{i3}. This mechanical impedance maintains the angle between the two links and imposes a joint torque given by (for leg i):

$$\begin{aligned} &\tau_{i3m} = -K_3 \Delta\theta_{i3} - B_3 \dot{\theta}_{i3} \\ &\Delta\theta_{i3} = \theta_{i3d}(t) - \theta_{i3}(t), \ \dot{\theta}_{i3}, \ \dot{\theta}_{i3d}(t), \ \theta_{i3}(t) \end{aligned} \quad (7)$$

where, τ_{i3m} is the joint effective torque, K_3 and B_3 are the coefficients of stiffness and viscous friction and θ_{i3d} and θ_{i3} are the planned and real trajectories.

3.3 Robot Body Model

Figure 2 presents the dynamic model for the hexapod body and foot-ground interaction. It is considered a robot body compliance because walking animals have a spine that allows supporting the locomotion with improved stability. In the present study, the robot body is divided in n identical segments (each with mass $M_b n^{-1}$) and a linear spring-damper system is adopted to implement the intra-body compliance:

$$\begin{aligned} &f_{ixH} = -\sum_{i'=1}^{u} \left(K_{xH} \Delta x_{iH,i'H} + B_{xH} \dot{\Delta} x_{iH,i'H} \right) \\ &\Delta x_{iH,i'H} = x_{iH} - x_{i'H}, \ \dot{x}_{iH}, \ \dot{x}_{i'H} \end{aligned} \quad (8a)$$

$$\begin{aligned} &f_{iyH} = -\sum_{i'=1}^{u} \left(K_{yH} \Delta y_{iH,i'H} + B_{yH} \dot{\Delta} y_{iH,i'H} \right) \\ &\Delta y_{iH,i'H} = y_{iH} - y_{i'H}, \ \dot{y}_{iH}, \ \dot{y}_{i'H} \end{aligned} \quad (8b)$$

where $(x_{i'H}, y_{i'H})$ are the hip coordinates and u is the total number of segments adjacent to leg i.

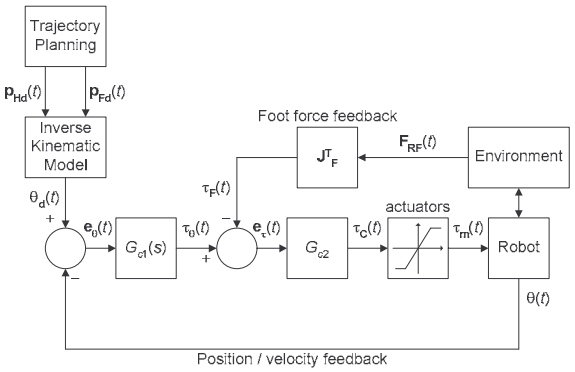

Fig. 3. Hexapod robot control architecture.

In this study, the parameters $K_{\eta H}$ and $B_{\eta H}$ ($\eta = \{x, y\}$) in the {horizontal, vertical} directions, respectively, are defined so that the body behaviour is similar to the one expected to occur on an animal (Table 1).

3.4 Foot-Ground Interaction Model

The contact of the i^{th} robot feet with the ground is modeled through a non-linear system (Silva, *et al*., 2003b) with damping $B_{\eta F}$ and stiffness $K_{\eta F}$ ($\eta = \{x, y\}$) in the {horizontal, vertical} directions, respectively (see Fig. 2), yielding:

$$\begin{aligned} &f_{ixF} = -K_{xF} \Delta x_{ixF} - B_{xF} \left(\dot{x}_{iyF} \right)^{v} \dot{x}_{ixF} \\ &\Delta x_{ixF} = x_{iF} - x_{iF0}, \ \dot{x}_{ixF}, \ \dot{x}_{iF}, \ x_{iF0} \end{aligned} \quad (9a)$$

$$\begin{aligned} &f_{iyF} = -K_{yF} \Delta y_{iyF} - B_{yF} \left(\dot{y}_{iyF} \right)^{v} \dot{y}_{iyF} \\ &\Delta y_{iyF} = y_{iF} - y_{iF0}, \ \dot{y}_{iyF}, \ \dot{y}_{iF}, \ y_{iF0} \end{aligned} \quad (9b)$$

where x_{iF0} and y_{iF0} are the coordinates of foot i touchdown and v is a parameter dependent on the ground characteristics. The values for the parameters $K_{\eta F}$ and $B_{\eta F}$ (Table 1) are based on the studies of soil mechanics (Silva, *et al*., 2003b).

3.5 Control Architecture

The general control architecture of the hexapod robot is presented in Fig. 3. On a previous work were demonstrated the advantages of a cascade controller, with *PD* position control and foot force feedback, over a classical *PD* with, merely, position feedback, particularly in real situations where we have non-ideal actuators with saturation and being also more robust for variable ground characteristics (Silva and Machado, 2003). Based on these results, in this study we evaluate the effect of different *FO* controller implementations for $G_{c1}(s)$, while for G_{c2} it is considered a simple *P* controller. For the *FO* algorithm we have:

$$G_{C1j}(s) = K_j s^{\alpha_j}, \quad 1 \le \alpha_j \le 1, \ j = 1,2,3 \quad (10)$$

where K_j is the gain and α_j is the fractional order.

In what concerns Eq. (10) it should be noted that the mathematical definition of a derivative of fractional order has been the subject of several different

approaches. For example, Eq. (11a) and Eq. (11b), represent the Laplace (for zero initial conditions) and the Grünwald-Letnikov definitions of the fractional derivative of order α of the signal $x(t)$:

$$D^{\alpha}[x(t)] = L^{-1}\{s^{\alpha} X(s)\} \tag{11a}$$

$$D^{\alpha}[x(t)] = \lim_{h \to 0} \left[\frac{1}{h^{\alpha}} \sum_{k=1}^{\infty} \frac{(-1)^k \Gamma(\alpha + 1)}{\Gamma(k+1)\Gamma(\alpha - k + 1)} x(t - kh) \right] \tag{11b}$$

where Γ is the gamma function and h is the time increment.

In this paper, for implementing the *FO* algorithm (Eq. (10)) it is adopted a discrete-time 4th-order Padé approximation (a_{ij}, $b_{ij} \in \Re$, $j = 1, 2, 3$) yielding an equation in the z-domain of the type:

$$G_{C1j}(z) \approx K_j \sum_{i=0}^{i=4} a_{ij} z^{-i} \Big/ \sum_{i=0}^{i=4} b_{ij} z^{-i} \tag{12}$$

where K_j is the controller gain.

4. MEASURES FOR PERFORMANCE EVALUATION

In mathematical terms we establish two global measures of the overall performance of the mechanism in an average sense. In this perspective, we define one index $\{E_{av}\}$ inspired on the system dynamics and another one $\{\varepsilon_{xyH}\}$ based on the trajectory tracking errors.

A first measure in this analysis is the mean absolute density of energy per travelled distance E_{av}. This index is computed assuming that energy regeneration is not available by actuators doing negative work, that is, by taking the absolute value of the power. At a given joint j (each leg has $m = 3$ joints) and leg i (since we are adopting a hexapod it yields $n = 6$ legs), the mechanical power is the product of the motor torque and angular velocity. The global index E_{av} is obtained by averaging the mechanical absolute energy delivered over the travelled distance L:

$$E_{av} = \frac{1}{L} \sum_{i=1}^{n} \sum_{j=1}^{m} \int_0^T \left| \tau_{ijm}(t) \cdot \dot{\theta}_{ij}(t) \right| dt \tag{13}$$

In what concerns the hip trajectory following errors we can define the index:

$$\varepsilon_{xyH} = \sum_{i=1}^{n} \sqrt{\frac{1}{N_S} \sum_{k=1}^{N_S} \left(\Delta x_{iH}^2 + \Delta y_{iH}^2 \right)}, \quad \Delta x_{iH} = x_H^d(k) - x_H^r(k), \quad \Delta y_{iH} = y_H^d(k) - y_H^r(k) \tag{14}$$

where N_S is the total number of samples for averaging purposes and $\{d, r\}$ indicate the i^{th} samples of the desired and real position, respectively.

In all cases the performance optimization requires the minimization of each index.

Table 1 System parameters

Robot model parameters		**Locomotion parameters**	
S_P	1 m	β	50%
L_{ij}, j=1,2	0.5 m	L_S	1 m
L_{i3}	0.1 m	H_B	0.9 m
O_i	0 m	F_C	0.1 m
M_b	88.0 kg	V_F	1 ms^{-1}
M_{ij}, j=1,2	1 kg	**Ground parameters**	
M_{i3}	0.1 kg	K_{xF}	1302152.0 Nm^{-1}
K_{xH}	10^5 Nm^{-1}	K_{yF}	1705199.0 Nm^{-1}
K_{yH}	10^4 Nm^{-1}	B_{xF}	2364932.0 Nsm^{-1}
B_{xH}	10^3 Nsm^{-1}	B_{yF}	2706233.0 Nsm^{-1}
B_{yH}	10^2 Nsm^{-1}	v	0.9

Table 2 Controller parameters

Joint 3:	**mechanical actuated**		**motor actuated**	
$\alpha_j = 0.4$	K_1	4200.0	K_1	3900.0
	K_2	400.0	K_2	500.0
	K_3	2.0	K_3	100.0
	B_3	0.5		
$\alpha_j = 0.5$	K_1	7200.0	K_1	7600.0
	K_2	800.0	K_2	1600.0
	K_3	0.5	K_3	240.0
	B_3	2.0		
$\alpha_j = 0.6$	K_1	1000.0	K_1	200.0
	K_2	200.0	K_2	50.0
	K_3	1.0	K_3	25.0
	B_3	2.0		
$\alpha_j = 0.7$	K_1	700.0	K_1	200.0
	K_2	200.0	K_2	25.0
	K_3	0.5	K_3	25.0
	B_3	0.5		
$\alpha_j = 0.8$	K_1	400.0	K_1	100.0
	K_2	200.0	K_2	40.0
	K_3	4.0	K_3	20.0
	B_3	3.5		

5. SIMULATION RESULTS

In this section we develop a set of simulations to analyse the performances of the different *FO* controller tuning during a periodic wave gait at a constant forward velocity V_F. For simulation purposes we consider the locomotion parameters, the robot body parameters and the ground parameters (supposing that the robot is walking on a ground of compact clay) presented in Table 1.

5.1 Controller Tuning Methodology

To tune the different controller implementations we adopt a systematic method, testing and evaluating several possible combinations of parameters, for all controller implementations. Therefore, we adopt the $G_{c1}(s)$ parameters that establish a compromise in what concerns the simultaneous minimisation of ε_{xyH} and E_{av} and a proportional controller G_{c2} with gain $Kp_j = 0.9$ ($j = 1, 2, 3$). Moreover, it is assumed high performance joint actuators with a maximum actuator torque in Eq. (6) of $\tau_{ijMax} = 400$ Nm.

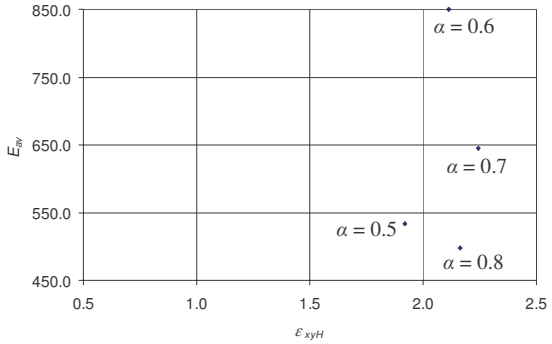

Fig. 4. Plots of ε_{xyH} *vs.* E_{av} for the different $G_{c1}(s)$ *FO* controller tuning, when establishing a compromise between the minimisation of ε_{xyH} and E_{av}, with $G_{c2} = 0.9$, joints 1 and 2 motor actuated and joint 3 mechanical actuated.

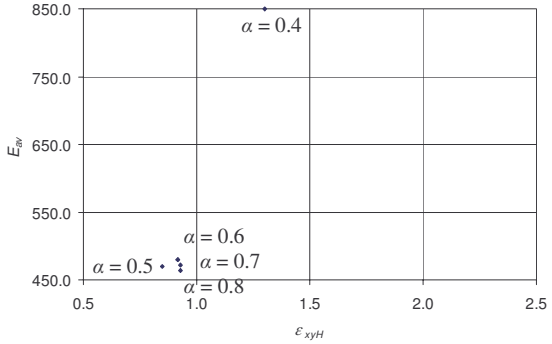

Fig. 5. Plots of ε_{xyH} *vs.* E_{av} for the different $G_{c1}(s)$ *FO* controller tuning, when establishing a compromise between the minimisation of ε_{xyH} and E_{av}, with $G_{c2} = 0.9$ and all joints motor actuated.

We start by considering that leg joints 1 and 2 are motor actuated and joint 3 is mechanical actuated. For this case we tune the *FO* joint controllers for different values of the fractional order α_j in the interval $-0.9 < \alpha_j < +0.9$ and $\alpha_j \neq 0.0$. Afterwards, we consider that joint 3 is also motor actuated, and we repeat the controller tuning procedure versus α_j. The controller parameters, for both cases, are presented in Table 2.

5.2 FO Algorithm Performance

Figure 4 presents the best controller tuning for different values of α_j when joint 3 is simple mechanical actuated. We observe that the value of $\alpha_j = 0.5$ presents the best compromise situation in what concerns the simultaneous minimisation of ε_{xyH} and E_{av}. For values of $\alpha_j = \{0.6, 0.7, 0.8\}$ the values of ε_{xyH} are similar and slightly higher than the corresponding value for $\alpha_j = 0.5$. Concerning the values of E_{av}, the minimum is obtained for $\alpha_j = 0.8$.

Figure 5 presents a similar chart for the case when all joints are motor actuated. As in the previous case, we observe that the value of $\alpha_j = 0.5$ presents the best compromise situation in what concerns the simultaneous minimisation of ε_{xyH} and E_{av}. For values of $\alpha_j = \{0.6, 0.7, 0.8\}$ the values of ε_{xyH} are E_{av} are slightly higher.

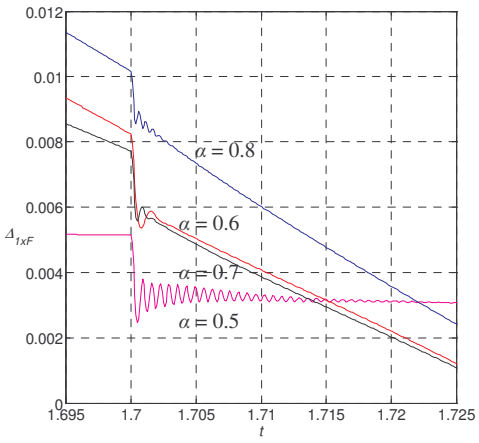

Fig. 6. Plots of Δ_{1xF} *vs.* t for $\alpha_j = \{0.5, 0.6, 0.7, 0.8\}$.

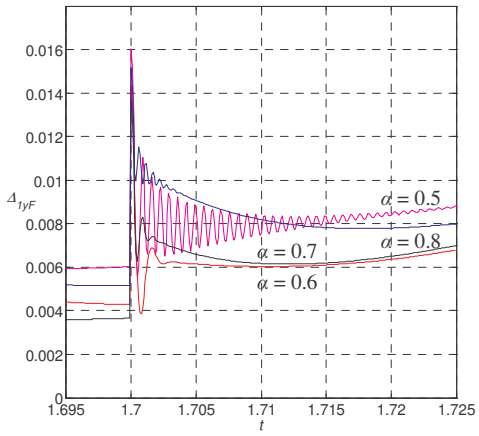

Fig. 7. Plots of Δ_{1yF} *vs.* t for $\alpha_j = \{0.5, 0.6, 0.7, 0.8\}$.

For values of $\alpha_j = \{0.1, 0.2, 0.3, 0.4\}$, the results are very poor and for $-0.9 < \alpha_j < -0.1$ and $\alpha_j = 0.9$, the hexapod locomotion resulted unstable. Furthermore, comparing Figures 4 and 5, we conclude that the best case correspond to leg joints being motor actuated.

In order to fully understand the different *FO* controller tuning, for the case of motor actuated joint 3, we analyse the response to a step foot disturbance, of amplitude $\Delta_{1yFd} = 0.01$ m, in the $y_{1Fd}(t)$ desired cartesian trajectory.

Figures 6 and 7 present the plots of Δ_{1xF} and Δ_{1yF} versus t for the values of the fractional order under consideration ($\alpha_j = \{0.5, 0.6, 0.7, 0.8\}$). Figure 7 reveals that the overshot is similar for all the values of α_j under consideration; nevertheless, for $\alpha_j = 0.5$ we have the higher settling time, while for $\alpha_j = 0.6$ we have the lower one.

Since the objective of the walking robots is to walk in natural terrains, in the sequel we test how the different controllers behave under distinct ground properties. Figures 8 and 9 present the time evolution of Δ_{1xF} and Δ_{1yF} versus α_j when the ground is of loose clay (Silva, *et al.*, 2003b). Through the comparison of these plots with the previous ones of Figures 6 and 7 we conclude that the controller responses are quite similar, meaning that these algorithms are robust to variations of the ground characteristics.

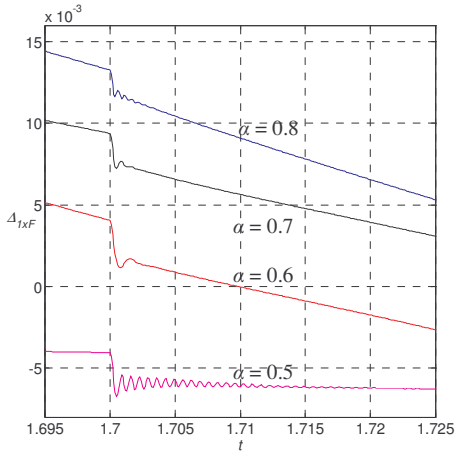

Fig. 8. Plots of Δ_{1xF} *vs.* t for $\alpha_j = \{0.5, 0.6, 0.7, 0.8\}$.

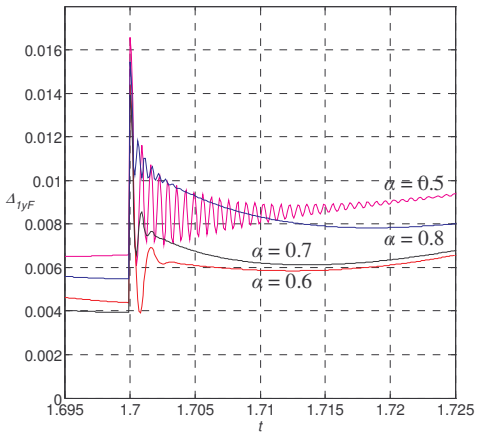

Fig. 9. Plots of Δ_{1yF} *vs.* t for $\alpha_j = \{0.5, 0.6, 0.7, 0.8\}$.

It is worth mentioning that in the case when joint 3 is mechanically actuated, the robot puts the toe tips in the ground, followed by the ankle. Both stay in this state during the feet support phase and, consequently, the robot walks supporting its body in link L_{i3}. On the contrary, when all joints are motor actuated, during the feet support phase, the robot walks in its toe tips. By other words, the hexapod supports itself in the extremity of link L_{i3}.

From the biological point of view both cases are important. Therefore, further study is necessary to understand more deeply how the behaviour change with the locomotion parameters.

6. CONCLUSIONS

In this paper we have compared the performance of different *FO* robot controller for joint leg control of a hexapod robot, both for the mechanical and motor actuated ankle joint.

In order to analyze the system performance two measures were defined based on the mean absolute density of energy per travelled distance and the hip trajectory errors. The leg response to a step disturbance in the feet trajectory is also considered for performance comparison purposes. The experiments reveal the superior performance of the *FO* controller for $\alpha_j \approx 0.5$ and a robot with all motor actuated joints.

The focus of the work presented has been on *FO* controllers with a pure derivative / integrative term. Presently we are studying the performance of the system in case we add several terms. Future work in this area will also address the study of the performance of these controllers when the hexapod is faced with variable ground conditions, obstacles and different locomotion parameters.

REFERENCES

Celaya, E. and Porta, J. (1995). Force-Based Control of a Six-Legged Robot on Abrupt Terrain Using the Subsumption Architecture. In: *Proc. of the Int. Conf. on Advanced Robotics*. pp. 413 – 419.

Collins, J. J. and Richmond, S. A. (1994). Hard-Wired Central Pattern Generators for Quadrupedal Locomotion. *Biological Cybernetics*, **71**, pp. 375 – 385.

Ferrell, C. (1995). A Comparison of Three Insect Inspired Locomotion Controllers. *Robotics and Autonomous Systems*, **16**, pp. 135–159.

Lee, K.-P., Koo, T.-W. and Yoon, Y.-S. (1998). Real-Time Dynamic Simulation of Quadruped Using Modified Velocity Transformation. In: *Proc. of the IEEE Int. Conf. on Robotics and Automation*. Belgium, pp. 1701 – 1706.

Martins-Filho, L. de S., Silvino, J. L., Resende, P. and Assunção, T. C. (2003). Control of Robotic Leg Joints – Comparing PD and Sliding Mode Approaches. In: *Proc. 6th Int. Conf. on Climbing and Walking Robots*. Italy, pp. 147–153.

McGeer, T. (1990). Passive Dynamic Walking. *Int. Journal of Robotics Research*, **9**, pp. 62–82.

Silva, M. F, and Machado, J. A. T. (2003). Position and Force Control of a Walking Hexapod. In: *Proc. of the 11th Int. Conf. on Advanced Robotics*. Portugal, pp. 1743–1748.

Silva, M. F., Machado, J. A. T. and Lopes, A. M. (2003a). Comparison of fractional and integer order control of an hexapod robot. In: *Proc. VIB 2003 – ASME Int. 19th Biennial Conf. on Mechanical Vibration and Noise*, USA.

Silva, M. F., Machado, J. A. T. and Lopes, A. M. (2003b). Position / Force Control of a Walking Robot. *Machine Intelligence and Robotic Control*, **5**, pp. 33 – 44.

Song, J., Low, K. H. and Guo, W. (1999). A Simplified Hybrid Force/Position Controller Method for the Walking Robots. *Robotica*, **17**, pp. 583–589.

Song, S.-M. and Waldron, K.J. (1989). *Machines that Walk: The Adaptive Suspension Vehicle*. The MIT Press.

Tsai, C.-R. and Lee, T.-T. (1998). A Study of Fuzzy-Neural Force Control for a Quadrupedal Walking Machine. *Journal of Dynamic Systems, Measurement and Control*, **120**, pp. 124–133.

Tsai, C.-R., Lee, T.-T. and Song, S.-M.. (1997). Fuzzy Logic Control of a Planetary Gear Type Walking Machine Leg. *Robotica*, **15**, pp. 533–546.